Check for updates

Geophysical Research Letters

RESEARCH LETTER
10.1029/2024GL110225

A Global Ocean Opal Ballasting–Silicate Relationship

B. B. Cael[1], C. Mark Moore[2], Joe Guest[3], Tereza Jarníková[3], Colleen B. Mouw[4], Chris Bowler[5,6], Edward Mawji[1], Stephanie A. Henson[1], and Corinne Le Quéré[3]

[1]National Oceanography Centre, Southampton, UK, [2]School of Ocean and Earth Science, University of Southampton, Southampton, UK, [3]School of Environmental Sciences, University of East Anglia, Norwich, UK, [4]University of Rhode Island, Graduate School of Oceanography, Narragansett, RI, USA, [5]Institut de Biologie de l'Ecole Normale Supérieure (IBENS), Ecole Normale Supérieure, CNRS, INSERM, Université PSL, Paris, France, [6]Stazione Zoologica Anton Dohrn, Naples, Italy

Key Points:

- Opal ballasting varies by more than a factor of six across ocean regions; calcium carbonate ballasting is uniform
- Silicate concentration predicts opal ballasting which suggests that the latter varies with diatom frustule thickness
- This emergent relationship's absence from a sophisticated biogeochemical model indicates it holds useful information for constraining models

Correspondence to:
B. B. Cael,
cael@noc.ac.uk

Citation:
Cael, B. B., Moore, C. M., Guest, J., Jarníková, T., Mouw, C. B., Bowler, C., et al. (2024). A global ocean opal ballasting–silicate relationship. *Geophysical Research Letters*, *51*, e2024GL110225. https://doi.org/10.1029/2024GL110225

Received 9 MAY 2024
Accepted 1 AUG 2024

Abstract Opal and calcium carbonate are thought to regulate the biological pump's transfer of organic carbon to the deep ocean. A global sediment trap database exhibits large regional variations in the organic carbon flux associated with opal flux. These variations are well-explained by upper ocean silicate concentrations, with high opal 'ballasting' in the silicate-deplete tropical Atlantic Ocean, and low ballasting in the silicate-rich Southern Ocean. A plausible, testable hypothesis is that opal ballasting varies because diatoms grow thicker frustules where silicate concentrations are higher, carrying less organic carbon per unit opal. The observed pattern does not fully emerge in an advanced ocean biogeochemical model when diatom silicification is represented using a single global parameterization as a function of silicate and iron. Our results suggest a need for improving understanding of currently modeled processes and/or considering additional parameterizations to capture the links between elemental cycles and future biological pump changes.

Plain Language Summary Opal, or hydrated silica, is taken up in the surface ocean by diatoms to construct their protective frustules. Another plankton type, coccolithophores, generate protective platelets from calcium carbonate. These two minerals, and thereby plankton types, play major roles in the global carbon cycle. The 'biological carbon pump' transfers carbon from the upper ocean to the ocean's depths, where it can stay for millenia. This process has influenced past atmospheric carbon dioxide concentrations and could also do so in the future. The transfer of carbon to the deep ocean is partially regulated by the amount of 'ballast' minerals in sinking particles, especially opal and calcium carbonate, which are denser and cause particles to sink faster and/or protect organic carbon from microbial consumption. We show that unlike calcium carbonate, opal's ballasting effect varies a great deal between different regions of the ocean. The variation in opal ballasting is well-explained by the upper-ocean concentration of silicate between these regions. This suggests a simple explanation: when silicate concentrations are high, diatoms grow thick frustules which actually results in lower carbon sinking per unit opal. Capturing this ballasting–silicate relationship in carbon cycle models may improve their ability to predict future biogeochemical cycles and climate.

1. Introduction

The biological carbon pump (BCP) entails the uptake, processing, and transfer of organic carbon to the deep ocean by biological processes. Particulate organic carbon (POC) and associated nutrients sinking out of the ocean's upper layer are gradually remineralized by grazing processes and microbial activity. The depth at which POC is remineralized determines the water mass that the resulting inorganic carbon enters, and thus the timescales of potential (re-)exposure to the atmosphere (Boyd et al., 2019; DeVries et al., 2012). Generally, the deeper POC penetrates into the ocean, the longer it is stored (Baker et al., 2022; Siegel et al., 2021). However, the mechanistic processes that underlie the considerable spatial and temporal variability in POC flux and remineralization (Bol et al., 2018; Cram et al., 2018) are still debated (Henson et al., 2022). One hypothesis posits that a portion of sinking POC is associated with 'ballast minerals', that is, calcium carbonate and biogenic silica generated by calcifying organisms and diatoms, respectively (Armstrong et al., 2001; Klaas & Archer, 2002). These minerals are thought to deepen the remineralization depth of POC either through protection of the POC, or by increasing the particles' excess density and thus sinking speed. Although the presence of ballast minerals has a strong statistical relationship with remineralization depth, a lack of mechanistic understanding introduces challenges for parameterizing ballasting in Earth system models, despite its potential to be an important component of carbon cycle-climate feedbacks (Barker et al., 2003; Heinze et al., 2019; Petrou et al., 2019).

© 2024. The Author(s).
This is an open access article under the terms of the Creative Commons Attribution License, which permits use, distribution and reproduction in any medium, provided the original work is properly cited.

19448007, 2024, 19, Downloaded from https://agupubs.onlinelibrary.wiley.com/doi/10.1029/2024GL110225 by University Of Southampton, Wiley Online Library on [15/10/2024]. See the Terms and Conditions (https://onlinelibrary.wiley.com/terms-and-conditions) on Wiley Online Library for rules of use; OA articles are governed by the applicable Creative Commons License

Our objectives here are to diagnose (a) the ballast effects of opal and calcium carbonate (in terms of the POC flux at a reference depth associated with a unit of opal or calcium carbonate flux), (b) the extent to which the ballasting effects vary among ocean regions, (c) the drivers of regional variations, and (d) whether variations in ballasting effects might be helpful for constraining global ocean biogeochemical models. To achieve these objectives, we apply a statistical model based on the robust log-normality of ocean particle fluxes (Cael et al., 2018, 2021) to a global sediment trap database (Mouw et al., 2016). We find that, while the majority of parameters of the statistical model remain relatively constant, the ballasting by opal varies by almost an order of magnitude between different regions. We discuss various possible mechanisms to explain this regional difference but identify one that is parsimonious, plausible, and experimentally testable: diatom frustule thickness varies with upper ocean silicate availability. We find that this relationship does not occur in a state-of-the-art ocean biogeochemical model (Buitenhuis et al., 2019), underscoring that the opal ballasting pattern that we uncover here is not produced ecosystem and particle processes as currently parameterized, and therefore that this relationship holds useful information for constraining ocean biogeochemical models.

2. Methods

2.1. Statistical Model

Following (Cael et al., 2018, 2021), our statistical model is derived from the log-normality of POC/PIC/PSi fluxes. This statistical model is based on the empirically validated (Cael, 2021; Cael et al., 2018, 2021) argument that (a) net primary production varies log-normally because multiple conditions need to be met in order for production to occur, and production cannot occur if any one of these conditions is not met, such that the 'law of necessary conditions' applies (Montroll & Shlesinger, 1982), (b) the export ratio of export production over net primary production is a variable quantity, and particle export out of the euphotic layer is equal to net primary production times this export ratio by definition, and (c) particle flux at a given depth is equal to particle export times the transfer efficiency to that depth, which is also a variable quantity. If the fluxes of particulate organic carbon ($\mathcal{F}_{\mathrm{POC}}$ (mgC m^{-2} d^{-1}—though all fluxes are implicitly non-dimensionalized in Equation 1 by dividing by 1 mg m^{-2} d^{-1}), particulate inorganic carbon ($\mathcal{F}_{\mathrm{PIC}}$ (mgC m^{-2} d^{-1}, i.e. calcium carbonate in units of C mass), and particulate silica ($\mathcal{F}_{\mathrm{PSi}}$ (mgSi m^{-2} d^{-1}, i.e. opal in units of Si mass), are log-normally distributed (Cael et al., 2021), and the latter both act in concert as ballasting minerals (i.e., organic carbon flux to a given depth can be facilitated by either or both minerals and does not necessarily require both), then they should approximately be related by an equation of the form (Cael et al., 2021)

$$\mathcal{F}_{\mathrm{POC}} = (\alpha_{\mathrm{PIC}}\,\mathcal{F}_{\mathrm{PIC}} + \alpha_{\mathrm{PSi}}\,\mathcal{F}_{\mathrm{PSi}})^{\gamma} z^{\Delta b}. \tag{1}$$

In Equation 1 α_{PIC} (dimensionless) is the organic carbon flux associated with a unit of inorganic carbon flux, α_{PSi} (gC/gSi) is the organic carbon flux associated with a unit of opal flux, and γ (dimensionless) is the degree of sub-/super-linearity in the scaling relationship between organic carbon fluxes and ballast mineral fluxes. The difference in flux attenuation between POC and ballast minerals is captured by $\Delta b = b - b_{bal}$, which is the difference between the exponents of the power-law profiles ((Martin et al., 1987)) of fluxes of POC and mineral ballasts. Equation 1 implicitly assumes that the PSi and PIC fluxes are attenuated with the same exponent. Equation 1 also does not account for POC flux not associated with mineral ballast, because these fluxes are implicitly assumed to be negligible at the deep measurement depths of interest here; this relationship is therefore likely invalid at shallow depths such as the base of the euphotic layer (though note we find no systematic depth dependency of the residuals in our analysis; see §3.1). Here z is normalized to a given reference depth z_0, for which we use 1 km. Our results are not affected by this choice. γ can be interpreted as the extent to which the effect of ballast minerals have 'diminishing returns' because if $\gamma < 1$ and increasingly so as $\gamma \to 0$, particles with for example, twice the ballast mineral loading will have less than twice the organic carbon content (γ can in principle be >1 but this is mechanistically implausible and is not seen in the observations). α_{PIC} and α_{PSi} can be interpreted as the organic carbon flux per unit of each ballast mineral flux at the reference depth; strictly speaking this is only true when $\gamma = 1$, but regardless of the value of γ the ratio of the α values captures the relative ballast effect per unit mass of each mineral (Note that Equation 1 is equivalent to the one given in (Cael et al., 2021), with Δb used here in replacement of b to make it explicit that this parameter captures the *difference* in vertical attenuation of organic carbon vs. ballast mineral fluxes, $\alpha_{\mathrm{PIC}} = \kappa^{1/\gamma}$ and $\alpha_{\mathrm{PSi}} = \beta\kappa^{1/\gamma}$ used in replacement of κ and β to make the ballast

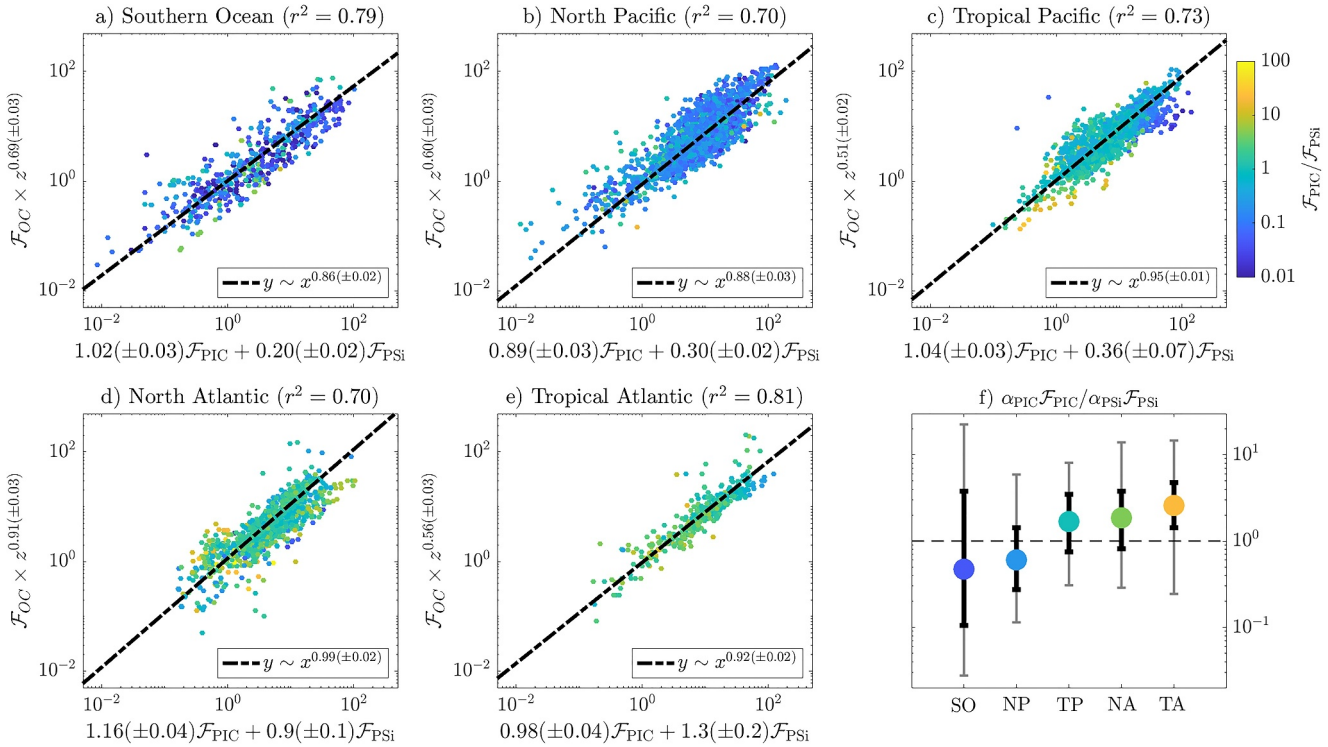

Figure 1. a-e) Scaling relationships corresponding to Equation 1 between organic carbon and ballast fluxes for the five regions considered here. Color indicates the PIC:PSi flux ratio. Parameter estimates are given on *x*- and *y*-axis labels. Units on both axes are mgC m^{-2} d^{-1}. Parameter values and uncertainties are estimated as described in the Methods. f) Median, interquartile range, and 95% range of ratio of POC flux at 1 km estimated to be associated with inorganic carbon versus opal (i.e., $\alpha_{PIC}\,\mathcal{F}_{PIC}/\alpha_{PSi}\,\mathcal{F}_{PSi}$) for each region. Dashed black line corresponds to equal organic carbon flux associated with each ballast mineral.

effect of each mineral explicit parameters, and a reference depth of 1 km used rather than 3,500 m because measurements of the full water column are considered rather than just near-bottom sediment traps.).

2.2. Sediment Trap Data

We utilized a global dataset of POC, PIC, and particulate silica (PSi) flux estimated from POC, PIC, and PSi concentration observations from sediment traps (Mouw et al., 2016). We only analyze coincident POC, PIC, and PSi flux measurements from sediment traps. Data were compiled from public repositories and directly from the literature. PIC fluxes are sometimes reported in $CaCO_3$ flux units, and PSi fluxes are sometimes reported in SiO_2 and $Si(OH)_4$ flux units; we converted these to PIC and PSi fluxes respectively using the ratio of their molar masses. The data set contains 15,792 individual POC flux estimates, measured on timescales of days to weeks, at 674 unique locations collected between 1976 and 2012; see Figure 1 in (Mouw et al., 2016). Most of the dataset (71%) was measured at ≥500 m, with the most common deployment depths between 1,000 and 1,500 m. 85% of the observations are concentrated in the Northern Hemisphere (For the two tropical regions spanning both hemispheres, 45% of the Tropical Atlantic data are from the Northern Hemisphere, whereas 87% of the Tropical Pacific data are from the Northern Hemisphere; thus the latter can essentially be considered representative of the Northern Tropical Pacific. Excluding the 258 (of 2,286) Southern Hemisphere data points from the Tropical Pacific region does not meaningfully affect our results.)

These data are split into five broad geographic regions. The Southern Ocean (SO) is defined here as south of 30°S, the North Pacific (NP) and Atlantic (NA) as north of 30°N, and the Tropical Pacific (TP) and Atlantic (TA) aas all data equatorward of 30° (There are few measurements in the Indian Ocean and these are included as part of the Pacific measurements; the Tropical Pacific regions is technically therefore the Tropical Indo-Pacific, though we refer to it as the Tropical Pacific because the measurements are predominantly from the Pacific Ocean.) The data from major time-series sites were excluded from our analyses, as the database is unavoidably very spatially biased, even without including these sites, and these locations would be vastly over-represented if included, such

19448007, 2024, 19, Downloaded from https://agupubs.onlinelibrary.wiley.com/doi/10.1029/2024GL110225 by University Of Southampton, Wiley Online Library on [15/10/2024]. See the Terms and Conditions (https://onlinelibrary.wiley.com/terms-and-conditions) on Wiley Online Library for rules of use; OA articles are governed by the applicable Creative Commons License

19448007, 2024, 19, Downloaded from https://agupubs.onlinelibrary.wiley.com/doi/10.1029/2024GL110225 by University Of Southampton, Wiley Online Library on [15/10/2024]. See the Terms and Conditions (https://onlinelibrary.wiley.com/terms-and-conditions) on Wiley Online Library for rules of use; OA articles are governed by the applicable Creative Commons License

that our global analysis would be largely dictated by the behavior of a few locations (the majority with low silicate concentrations, furthermore). Excluding these locations, the database includes 768/2274/2286/1327/504 co-located measurements of $\mathcal{F}_{POC}$, $\mathcal{F}_{PIC}$, and $\mathcal{F}_{PSi}$ in the SO/NP/TP/NA/TA respectively.

2.3. Statistical Analysis

Equation 1 is fit to the data from each region following the regression procedure in (Cael et al., 2021). The $(\alpha_{PSi}/\alpha_{PIC}, \Delta b)$ that yields the best fit, using a scaling relationship of the form $y \propto x^{\gamma}$, between $\mathcal{F}_{POC} z^{\Delta b}$ and $\mathcal{F}_{PIC} + \frac{\alpha_{PSi}}{\alpha_{PIC}} \mathcal{F}_{PSi}$ is identified. Major axis type II regression is used to account for the fact that uncertainties exist on both the x- and y-axis. Multiplicative (i.e., relative rather than absolute) errors are assumed, given that particle fluxes scale with one another and are log-normally distributed. Parameter uncertainties are calculated via bootstrap resampling (Efron & Tibshirani, 1986) with 1,000 bootstrap reiterations and reported as the median absolute deviation amongst bootstrap ensemble members.

To estimate the opal ballasting for each individual measurement, Equation 1 is recast into

$$\alpha_{PSi} = \frac{1}{\mathcal{F}_{PSi}} \left(\left(\mathcal{F}_{POC} z^{-\Delta b} \right)^{1/\gamma} - \alpha_{PIC} \mathcal{F}_{PIC} \right). \quad (2)$$

The measured fluxes of POC, PIC, and PSi, and the measurement depth, along with a representative global value for γ, Δb, and α_{PIC} (here we use the mean across regions as these other parameters are fairly constant between regions, see §3) are then used in Equation 2 to estimate α_{PSi}. This estimate of α_{PSi} is then compared to co-located upper ocean silicate concentrations ([Si] (μmol/kg),) to test the hypothesis that higher [Si] values are associated with lower α_{PSi} values [Si] values were taken from the World Ocean Atlas 2018 (Garcia et al., 2019). The 80 m depth at which [Si] is considered here was selected as the depth at which the Spearman rank correlation between [Si] at that depth and the inferred α_{PSi} at the same latitude and longitude is a maximum. For 80 m, the correlation is 0.68. Our results are not sensitive to this choice; the correlation for all depths 0–500 m is $\geq$0.65. The logarithm of α_{PSi} is then regressed against the logarithm of [Si] (at 80 m) using the second-order polynomial of the form $y = p_2 x^2 + p_0$, which approximately captures the nonlinear relationship between $\log(\alpha_{PSi})$ and log ([Si]) in §3.3. Including a $p_1 x$ term made no difference.

2.4. Numerical Model

A global ocean biogeochemical model is used to test if the properties inferred using the database emerge in the current generation of models. We use the NEMO-PlankTOM12 model which represents explicitly 12 Plankton Functional Types (PFTs), six phytoplankton types (picophytoplankton, N_2-fixers, diatoms, *Phaeocystis*, and other mixed-phytoplankton), five zooplankton (protozooplankton, mesozooplankton, crustacean and gelatinous macrozooplankton, and pteropods) and bacteria (Buitenhuis et al., 2019, 2023; Le Quéré et al., 2016; Wright et al., 2021). All PFTs are represented using vital parameters of growth and loss rates based on available observations, and interact with each other using food preferences generally based on size. Growth rates depend on temperature and nutrient availability.

The model includes a full silicon cycle, with its dissolved, biogenic and detrital pools. The Si:C ratio within diatoms increases with iron stress and silicate availability as in (Aumont et al., 2015). Loss processes of diatoms produce sinking particulate silica, therefore the PSi:POC ratio is dependent on both iron and silica availability, as well as diatom concentration, grazing, and dissolution rates. Sinking of organic matter is a function of the ballasting density of the particles. A full description of the equations and parameters is provided in the PlankTOM12 manual (Buitenhuis et al., 2023). The model is embedded in the NEMOv3.6 general ocean circulation model, and is forced with NCEP reanalysis data (Saha et al., 2010). The model includes an optimization of global parameters to reproduce the size and vertical profiles of the observed organic carbon, opal and calcium carbonate fluxes presented here. This optimization was conducted by modifying the remineralization rate of silica, the dissolution rate of calcite, and the remineralisation rate of POC, until the global model POC, PSi and PIC fluxes reproduced the global median of the observations as a function of depth. We conducted sensitivity simulations with the variable Si:C ratio to test the effect on PSi:POC of modifying model parameters. In addition to the optimized baseline simulation, we present two extremes, one where the Si:C ratio is fixed by removing its dependence on silicate and iron concentrations, and one where the maximum Si:C is doubled from optimal model value (the range between maximum and

19448007, 2024, 19, Downloaded from https://agupubs.onlinelibrary.wiley.com/doi/10.1029/2024GL110225 by University Of Southampton, Wiley Online Library on [15/10/2024]. See the Terms and Conditions (https://onlinelibrary.wiley.com/terms-and-conditions) on Wiley Online Library for rules of use; OA articles are governed by the applicable Creative Commons License

Table 1
Parameter Estimates and Uncertainties (Median Absolute Deviation) for Each Region

Region	α_{PIC}	α_{PSi}	γ	Δb
Southern Ocean	1.02 ± 0.03	0.20 ± 0.02	0.86 ± 0.02	0.69 ± 0.03
North Pacific	0.89 ± 0.03	0.30 ± 0.02	0.88 ± 0.03	0.60 ± 0.03
Tropical Pacific	1.04 ± 0.03	0.36 ± 0.07	0.95 ± 0.01	0.51 ± 0.02
North Atlantic	1.16 ± 0.04	0.9 ± 0.1	0.99 ± 0.02	0.91 ± 0.03
Tropical Atlantic	0.98 ± 0.04	1.3 ± 0.2	0.92 ± 0.02	0.56 ± 0.03

Note. These are calculated from the regression method visualized in Figure 1a–1e

minimum Si:C is increased from 6 to 12) and the half-saturation concentration regulating the Si concentration at which this effect takes place is halved (from 20 to 10 μmol/L). Those ranges are chosen to encompass possible extremes based on the existing model parameterisation.

3. Results and Discussion

3.1. Regional Scaling Relationships

Figure 1 shows the fit of Equation 1 to the sediment trap data in each region. In each case, $\mathcal{F}_{POC}$ is well-predicted from ballast fluxes, with $r^2 = 0.70$–0.81. The ballast effect of opal, α_{PSi}, has a coefficient of variation of 77%, and varies by more than a factor of six between 1.3±0.2 gC/gSi in the Tropical Atlantic to 0.20±0.02 gC/gSi in the Southern Ocean (Table 1). In other words, in the Tropical Atlantic 1 mgSi m^{-2} d^{-1} of opal flux carries more than six times more organic carbon flux at 1 km than 1 mgSi m^{-2} d^{-1} of opal flux in the Southern Ocean. The highest α_{PSi} values are found in the Atlantic, then the Pacific and then the Southern Ocean. Within the Atlantic and Pacific Oceans, the tropical regions have larger α_{PSi} values than the Northern regions (Figure 1f). Altogether there appears to be a very large difference in the Si associated mineral ballasting between different ocean regions, with potentially large implications for ocean biogeochemical cycling. By comparison, the parameters α_{PIC} and γ, and Δb vary less between regions, with coefficients of variation of 10%, 6%, and 24% respectively (these parameters are discussed below).

Despite the much smaller α_{PSi} values in the Southern Ocean and North Pacific, the far larger $\mathcal{F}_{PSi}$ fluxes in these regions mean that opal carries more POC flux at 1 km than PIC for a majority of measurements in those regions (Figure 1f), as quantified by a $\alpha_{PIC}\,\mathcal{F}_{PIC}/\alpha_{PSi}\,\mathcal{F}_{PSi}$ ratio of <1. In the other three regions, calcium carbonate carries more POC flux at 1 km, that is, there is a $\alpha_{PIC}\,\mathcal{F}_{PIC}/\alpha_{PSi}\,\mathcal{F}_{PSi}$ ratio >1, for a majority of measurements, as has often been reported in the literature (Armstrong et al., 2001; Francois et al., 2002; Klaas & Archer, 2002; Wilson et al., 2012). The large variability of this ratio between measurements in all regions underscores that both ballast minerals play important roles; the interquartile range of $\alpha_{PIC}\,\mathcal{F}_{PIC}/\alpha_{PSi}\,\mathcal{F}_{PSi}$ spans values below and above one for all regions besides the tropical Pacific.

Parameters other than α_{PSi} are fairly uniform across regions and change in plausible ways in light of the processes controlling the biological pump. α_{PIC} is nearly constant between regions, consistent with PIC either increasing particles' excess density or protecting POC similarly between regions. γ is slightly < one in all regions except the North Atlantic, but only slightly so, indicating some degree of 'diminishing returns' on the effect of ballast minerals, but not enough to make as large a difference to POC fluxes as variations in α_{PSi}. Δb is higher at higher latitudes. If one assumes that regional variations in Δb are predominantly due to variations in the attenuation of $\mathcal{F}_{POC}$, that is, that the spatial variations in the vertical attenuation of ballast fluxes are negligible compared to those of organic carbon fluxes, this observation is consistent with some sediment-trap derived patterns for b (Henson et al., 2012). These regional variations in Δb are enough to make an appreciable difference in $\mathcal{F}_{POC}$ fluxes at the seafloor—for example, for the mean ocean depth of $z = 3682$m (Charette & Smith, 2010), the smallest Δb yields a value of $(z/z_0)^{\Delta b} = 1.9$, whereas the largest Δb value yields 3.3. However, because the spatial variations in flux attenuation are highly uncertain and sometimes contrasting between studies (Henson et al., 2012; Marsay et al., 2015), we do not interpret these variations here; we instead focus on the larger variations in α_{PSi}.

Note that we do not find systematic behavior with depth in the residuals, which suggests that a power-law approximation of flux attenuation with depth is suitable for our analysis. We do not consider the variations in these parameters further.

3.2. Possible Mechanisms

A simple and arguably parsimonious explanation for the regional variations in α_{PSi} is that variations in α_{PSi} are determined by upper ocean silicate concentrations ([Si], μmol/kg). Indeed [Si] is lowest in the surface waters of the Atlantic and highest in the Southern Ocean, due to the interaction of the meridional overturning circulation with both the temperature dependent long remineralization length scale of Si and high Si:N uptake ratios in the surface Southern Ocean (Gnanadesikan, 1999; Holzer et al., 2014; Sarmiento et al., 2004, 2007). Globally Si is largely trapped in the Southern Ocean (Holzer et al., 2014) because of high production and export of PSi, which is

19448007, 2024, 19, Downloaded from https://agupubs.onlinelibrary.wiley.com/doi/10.1029/2024GL110225 by University Of Southampton, Wiley Online Library on [15/10/2024]. See the Terms and Conditions (https://onlinelibrary.wiley.com/terms-and-conditions) on Wiley Online Library for rules of use; OA articles are governed by the applicable Creative Commons License

largely regenerated at depths below the northward flowing Antarctic intermediate and sub-Antarctic mode waters (AAIW/SAMW) (Sarmiento et al., 2007). Outside the Southern Ocean, the Atlantic is partly filled with preformed Si carried by the upper branch of the overturning circulation, which is ventilated by AAIW/SAMW formed within the relatively Si-depleted lower latitudes of the Southern Ocean (Sarmiento et al., 2004), and the Pacific is partly filled by the lower branch, which is ventilated by the relatively Si-rich higher latitudes in the Southern Ocean. Furthermore, tropical regions in the Atlantic and Pacific are more Si-depleted than regions higher to the north because some ventilation of deep waters occurs at high latitudes, even in the Pacific (Qiu & Huang, 1995). As a result, Atlantic diatoms grow in the most Si-depleted conditions and Southern Ocean diatoms grow in the most Si-replete conditions, with tropical diatoms growing in intermediate Si concentations. The more Si-deplete the conditions in which diatoms grow, the less opportunity diatoms have to meet or exceed their minimum quota of silica. This will tend to lead to lower Si:C stoichiometry for diatoms in more Si-deplete conditions, meaning thinner-frustuled diatoms of a given size and/or larger diatoms. This is because opal is predominantly contained in diatoms' frustules, whereas carbon is predominantly contained in diatoms' interiors. Thus for two diatoms of the same size, the one with the thicker frustule will carry less organic C per unit Si as it sinks; similarly for two diatoms with the same frustule thickness, the smaller one will carry less organic C per unit Si as it sinks. If opal ballasting is due to intact diatom frustules carrying organic carbon downwards as they sink, then thinner frustules, and/or larger diatoms, will correspond to more organic carbon carried per unit opal, and hence larger α_{PSi}. Diatoms in the Southern Ocean, and to a lesser extent in the (North) Subarctic Pacific, will thus be expected to have more ability to make thicker frustules in order to protect themselves from grazers, as observed (Assmy et al., 2013; Pančić et al., 2019), which results in higher Si:C ratios and lower α_{PSi} values. We thus hypothesize that there should be a negative relationship between α_{PSi} and [Si] (see §3.3).

Several other factors may complicate this simple explanation for regional variation in α_{PSi}. Different diatom taxa are characterized by different morphologies, with widely varying sizes and opal frustule pattern variations (Round et al., 1990). Different diatom species also exhibit specific biogeographies, inhabiting different ocean regions (Malviya et al., 2016; Tréguer et al., 2018). Sporulation of diatoms, especially of those abundant in the Southern Ocean such as *Chaetoceros*, may also influence the Si:C of organic material sinking into the deep sea (Armand et al., 2008). The different compositions of diatom communities in different oceanic regions may therefore impact opal ballasting, but may also in turn be influenced by the global availability of Si (§3.3). Furthermore, the Si content of diatom frustules can be impacted by environmental conditions other than [Si]. Silicification of diatoms is tightly linked to the cell cycle of growth, with Si uptake primarily occurring during the G2 interphase (Martin-Jézéquel et al., 2000). If the availability of other nutrients needed for cell growth (nitrate, phosphate, or iron) or other external growth conditions slow or prolong the G2 phase of the cell cycle in diatoms, silicification and diatom ballast increases. It has also been reported that increased grazing pressure may also lead to more heavily silicified diatoms (Pondaven et al., 2007) presumably as a mechanism for organisms to enhance their protection from grazing losses. In contrast, Si deficiency is the only condition that acts to reliably lower the silica content of the diatom cell wall (Brzezinski et al., 1990). All these factors are likely to impact the formation and degradation of particles. Fecal pellets can also contribute appreciably to POC fluxes and their stoichoimetry is necessarily reflective of their prey (Ducklow et al., 2001), so the selective grazing of diatoms of different frustule thicknesses (Ryderheim et al., 2022) and the relative balance of fecal pellets and aggregates in total POC fluxes will also play a role. Additionally, dust deposition is known to vary between regions and may further affect particles directly by being incorporated as lithogenic ballast (n.b. These are not collated in the (Mouw et al., 2016) database) or indirectly by supplying nutrients such as iron and thereby influencing phytoplankton communities.

Of these additional factors, there has been particular previous focus on the observed enhanced silicification of diatoms in response to iron limitation (Brzezinski et al., 2003; Franck et al., 2000; Hutchins & Bruland, 1998; Takeda, 1998). This mechanism has been invoked to explain higher organic carbon export out of the upper ocean in iron-depleted (Brzezinski et al., 2015) and silicate-rich waters (Arteaga et al., 2019), as well as higher silicate burial in iron-depleted waters (Pichevin et al., 2014), alongside contributing to the higher Si:N export ratios observed in the SO (Sarmiento et al., 2004). Iron limitation dependent enhanced silicification could potentially produce α_{PSi} variations, because iron limitation would lead to thick diatom frustules, hence potentially lowering organic carbon per unit Si and hence α_{PSi}. At global scales, surface silicate concentrations will generally be anticorrelated with iron limitation (Browning & Moore, 2023), although the high latitude North Atlantic represents a possible exception (see below). Consequently we cannot currently discount some iron dependence contribution to the observed global scale patterns in α_{PSi}, however, we consider a direct silicate availability based

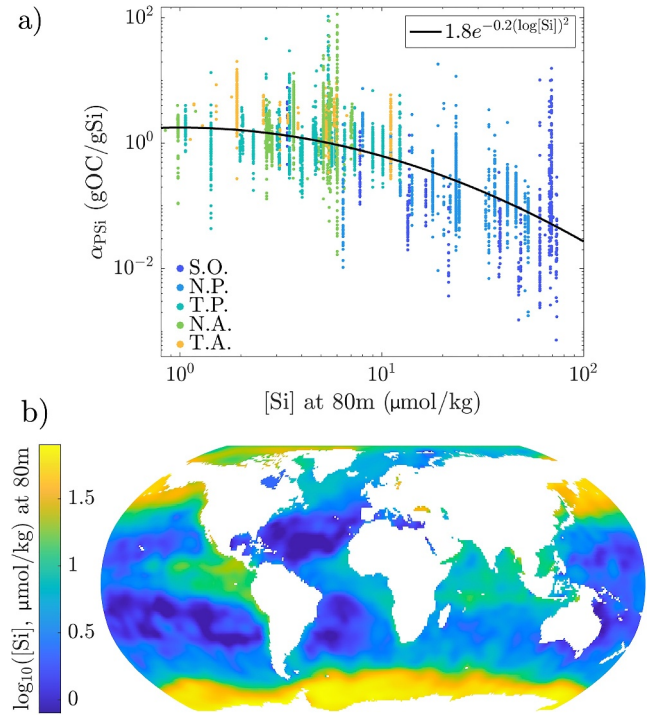

Figure 2. (a) Opal ballasting coefficient as estimated by Equation 2 (Methods) vs. silicate concentration at 80 m. Black line indicates empirical fit. (b) Annual mean logarithmic silicate concentration at 80 m in the World Ocean Atlas.

mechanism more plausible and parsimonious for several reasons. First, although iron limitation likely promotes enhanced silicification in diatoms, high silicate would still be necessary to supply the silicate uptake required for such increased silicification. Second, even in the absence of iron limitation, there are potential ecological advantages to enhanced silicification when silicate is abundant, for example, as a protection against grazing (). Third, the North Atlantic is known to be iron-limited to some degree (Browning & Moore, 2023), but we find a high α_{PSi} for that region, associated with the low silicate concentrations there (§3.3). Fourth, the model we analyze in §3.4 includes a parameterisation for the iron dependence mechanism but does not reproduce the observed α_{PSi}-[Si] relationship.

3.3. Silicate–Opal Ballasting Relationship

To test for a relationship between α_{PSi} and [Si] more quantitatively, we use Equation 2 to estimate α_{PSi} for each sediment trap measurement. For (α_{PIC}, Δb and γ) we use the means over the five regions (=1.02, 0.65, 0.92 respectively). Our results are not sensitive to these parameter values. We then compare these estimates to the co-located [Si] (at 80 m depth). Figure 2a shows that the estimated α_{PSi} decreased from a value of ~1.8 when [Si]→0, to small values as [Si] becomes large. This relationship is approximately described by the function $\alpha_{PSi} = 1.8e^{-0.2(\log[Si])^2}$ ($r^2 = 0.49$, $p \ll 0.01$). Decreasing α_{PSi} with increasing [Si] is consistent with the direct Si dependence hypothesis presented above, as low-[Si] regions would be expected to result in thinner diatom frustules and hence diatoms with more organic carbon per unit Si, with the opposite being the case for high-[Si] regions.

Note that it has also been shown that lower silicate concentrations are associated with higher export ratios (export production over net primary production) in the Southern Ocean (Arteaga et al., 2018; Britten et al., 2017), which has been attributed to opal ballasting. These results are consistent with but distinct from the α_{PSi}-[Si] relationship we present here, because they concern the ratio of organic carbon export out of the upper ocean to net primary production rather than organic carbon flux to silica flux below the upper ocean. Taken together these findings suggest that silicate-enriched waters have lower export ratios and lower organic carbon fluxes carried to depth per silica flux, both due to less effective opal ballasting.

19448007, 2024, 19, Downloaded from https://agupubs.onlinelibrary.wiley.com/doi/10.1029/2024GL110225 by University Of Southampton, Wiley Online Library on [15/10/2024]. See the Terms and Conditions (https://onlinelibrary.wiley.com/terms-and-conditions) on Wiley Online Library for rules of use; OA articles are governed by the applicable Creative Commons License

19448007, 2024, 19, Downloaded from https://agupubs.onlinelibrary.wiley.com/doi/10.1029/2024GL110225 by University Of Southampton, Wiley Online Library on [15/10/2024]. See the Terms and Conditions (https://onlinelibrary.wiley.com/terms-and-conditions) on Wiley Online Library for rules of use; OA articles are governed by the applicable Creative Commons License

3.4. Model Simulation

To test for the capacity of the NEMO-PlankTOM12 model to reproduce the observed [Si]-α_{PSi}, we sample the model analogously to how the real ocean has been sampled and repeat the same analysis on the pseudo-observations. Note that this exercise can provide evidence as to whether or not the observed relationship is caused by ecosystem and particle proesses as currently parameterized, but cannot validate our frustule thickness hypothesis. Specifically, we draw $\mathcal{F}_{POC/PIC/PSi}$ values at the 1,000 m reference depth at the same latitudes, longitudes, and months for which we have sediment trap measurements from monthly model output, using a randomly selected model year, 2000. Neither sub-monthly nor interannual variations should affect the relationship we investigate here. We also draw corresponding [Si] values at 80 m depth. We then repeat the analysis from §2.3 on these data.

When Si:C sensitivity to nutrient concentrations is turned off in the model, we find a weak relationship between model [Si] and inferred α_{PSi}, with a correlation coefficient of −0.13 (compared to −0.68 for the observations). When the standard Si:C sensitivity is used, we find a slightly stronger relationship (correlation of −0.14), but still much weaker than in the observations. Even the enhanced Si:C sensitivity returns a relationship that is still below the observations (correlation of −0.22). Thus the observed strong negative [Si]-α_{PSi} relationship is not found in the model. A full range of model sensitivity has not been performed, and modeled ecosystem composition, and in particular the relative concentration of diatoms, could affect those results. The weak dependence of α_{PSi} on [Si] may be explained by other factors discussed above that the model resolves, such as the balance of fluxes by fecal pellets versus aggregates or dust deposition. However, the absence of a clear strong relationship between [Si] and α_{PSi} in the model pseudo-observations suggests that the observed α_{PSi}-[Si] relationship may not be caused by ecosystem and particle processes as currently parameterized, and that the observed relationship therefore includes useful novel information for constraining and improving ocean biogeochemical models. As α_{PSi} quantifies the organic carbon fluxes carried by silica fluxes, the large observed variation in α_{PSi} suggests that correctly parameterizing the processes that produce the observed α_{PSi}-[Si] relationship could substantially improve models' ability to simulate the present-day biological pump and to predict its future changes. The observed α_{PSi}-[Si] relationship is in this sense a novel piece of evidence to constrain models' representation of ecosystem—carbon export relationship. This constraint is particularly valuable as ecosystem complexity is currently becoming increasingly well-represented within carbon cycle models. Validation of models using such emergent relationships can help improve the representation of the biological carbon pump, which should help reduce the large model spread in projections of biological pump changes.

3.5. Conclusion

Altogether these results suggest that the ballasting effect by opal varies a great deal in different parts of the ocean, and that much of this variation can be explained by local surface ocean silicate concentrations. We argue that the most parsimonious explanation of this pattern is that diatom communities in silicate-rich regions have more fustrule mass per unit interior mass than those in silicate-depleted regions. If diatom frustules carry the organic carbon inside them as they sink, such a silicate concentration–opal ballasting relationship may occur irrespective of whether this is due to physiological plasticity or ecological selection, differences in diatom size or morphology, and whether the change in thickness is in response to metabolic constraints linked with availability of other nutrients or top-down effects linked to grazing pressure from zooplankton.

One important aspect to demonstrated here is that variable stoichiometry alone may not be sufficient to parameterize the frustule thickness mechanism that we hypothesize to cause the relationship between α_{PSi} and [Si]. Diatoms' silicate uptake ratio relative to other elements is dependent on silicate concentrations (Brzezinski et al., 2011; Jin et al., 2006; Marchetti et al., 2010), meaning higher [Si] can lead to higher diatom Si:C ratios and hence lower α_{PSi}. Some models also incorporate the effect of iron concentrations on silicate uptake (Matsumoto et al., 2013; Pasquier & Holzer, 2017), and some models such as the one we analyze here (Pasquier & Holzer, 2017; Wright et al., 2021) incorporate both Si and Fe effects simultaneously. The model we analyze here incorporates stoichiometric variations but still does not reproduce the observed α_{PSi}-[Si] relationship. This suggests that this observed relationship is not only due to variations in diatom stoichiometry, but also how diatom Si and C are incorporated into particles and remineralized as particles sink. This could be explained, as described in §3.2, by intact diatom frustules within sinking particles carrying organic carbon within them as they sink. In any case, the results in §3.4 suggest that not only the variations in diatom stoichiometry and frustule thickness, but also

the effect of these variations on particle sinking and/or remineralization dynamics, need to be better parameterized to capture the observed α_{PSi}-[Si] relationship.

As mentioned above, other factors may also play a role, such as the grazing protection provided by thicker frustules (Assmy et al., 2013; Ryderheim et al., 2022), which could also in principle be parameterized. The very large gradients in silicate concentration in the upper ocean (Figure 2b) suggest that the inclusion of this phenomenon could generate large changes for historical estimates and future projections of carbon export, particularly if this phenomenon substantially influences the distribution of Si (Griffiths et al., 2013; Matsumoto et al., 2002; Matsumoto & Sarmiento, 2008). Note however that the relationship in Figure 2a also includes a great deal of variability, which would have to be accounted for in such a parameterization for example, by a transformation bias correction (Beauchamp & Olson, 1973). This variability is not surprising in light of the known variability in POC fluxes, the characteristics of which inform our statistical model (Cael et al., 2018, 2021). Such a parameterization also constitutes a hypothesis which could be tested experimentally and further refined with measurements of diatoms' stoichiometry, frustule thickness, and size, in different regions and/or across silicate concentration gradients.

Data Availability Statement

The data used for this study are available from (Garcia et al., 2019; Mouw et al., 2016) and the code for their analysis is available at (Cael, 2024). Numerical model documentation and output are available at (Buitenhuis et al., 2023).

Acknowledgments
We thank Angelicque White, Thomas Kiørboe, and Ken Andersen for useful discussions, and Benoît Pasquier and an anonymous reviewer for their constructive feedback. Cael, Henson and Jarníková acknowledge support by the National Environmental Resarch Council (NERC) Grant NE/T010622/1 CELOS (Constraining the EvoLution of the southern Ocean carbon Sink). Cael, Guest, Henson, and Le Quéré acknowledge support from Schmidt Sciences via the Virtual Earth System Research Institute project CALIPSO. Le Quéré acknowledges support from the NERC Grant NE/V011103/1 Marine Frontiers. Guest acknowledges support from the Royal Society Grant RP.R1.191063. Bowler acknowldges support from the European Research Council (ERC) under the European Union's Horizon 2020 research and innovation programme (Diatomic; grant agreement No. 835067).

References

Armand, L. K., Cornet-Barthaux, V., Mosseri, J., & Queguiner, B. (2008). Late summer diatom biomass and community structure on and around the naturally iron-fertilised kerguelen plateau in the southern ocean. *Deep Sea Research Part II: Topical Studies in Oceanography*, *55*(5–7), 653–676. https://doi.org/10.1016/j.dsr2.2007.12.031

Armstrong, R. A., Lee, C., Hedges, J. I., Honjo, S., & Wakeham, S. G. (2001). A new, mechanistic model for organic carbon fluxes in the ocean based on the quantitative association of poc with ballast minerals. *Deep Sea Research Part II: Topical Studies in Oceanography*, *49*(1–3), 219–236. https://doi.org/10.1016/s0967-0645(01)00101-1

Arteaga, L. A., Haetjens, N., Boss, E., Johnson, K. S., & Sarmiento, J. L. (2018). Assessment of export efficiency equations in the southern ocean applied to satellite-based net primary production. *Journal of Geophysical Research: Oceans*, *123*(4), 2945–2964. https://doi.org/10.1002/2018jc013787

Arteaga, L. A., Pahlow, M., Bushinsky, S. M., & Sarmiento, J. L. (2019). Nutrient controls on export production in the southern ocean. *Global Biogeochemical Cycles*, *33*(8), 942–956. https://doi.org/10.1029/2019gb006236

Assmy, P., Smetacek, V., Montresor, M., Klaas, C., Henjes, J., Strass, V. H., et al. (2013). Thick-shelled, grazer-protected diatoms decouple ocean carbon and silicon cycles in the iron-limited antarctic circumpolar current. *Proceedings of the National Academy of Sciences*, *110*(51), 20633–20638. https://doi.org/10.1073/pnas.1309345110

Aumont, O., Ethé, C., Tagliabue, A., Bopp, L., & Gehlen, M. (2015). Pisces-v2: An ocean biogeochemical model for carbon and ecosystem studies. *Geoscientific Model Development*, *8*(8), 2465–2513. Retrieved from https://doi.org/10.5194/gmd-8-2465-2015

Baker, C. A., Martin, A. P., Yool, A., & Popova, E. (2022). Biological carbon pump sequestration efficiency in the north atlantic: A leaky or a long-term sink? *Global Biogeochemical Cycles*, *36*(6), e2021GB007286. https://doi.org/10.1029/2021gb007286

Barker, S., Higgins, J. A., & Elderfield, H. (2003). The future of the carbon cycle: Review, calcification response, ballast and feedback on atmospheric co2. *Philosophical Transactions of the Royal Society of London,Series A: Mathematical, Physical and Engineering Sciences*, *361*(1810), 1977–1999. https://doi.org/10.1098/rsta.2003.1238

Beauchamp, J. J., & Olson, J. S. (1973). Corrections for bias in regression estimates after logarithmic transformation. *Ecology*, *54*(6), 1403–1407. https://doi.org/10.2307/1934208

Bol, R., Henson, S. A., Rumyantseva, A., & Briggs, N. (2018). High-frequency variability of small-particle carbon export flux in the northeast atlantic. *Global Biogeochemical Cycles*, *32*(12), 1803–1814. https://doi.org/10.1029/2018gb005963

Boyd, P. W., Claustre, H., Levy, M., Siegel, D. A., & Weber, T. (2019). Multi-faceted particle pumps drive carbon sequestration in the ocean. *Nature*, *568*(7752), 327–335. https://doi.org/10.1038/s41586-019-1098-2

Britten, G. L., Wakamatsu, L., & Primeau, F. W. (2017). The temperature-ballast hypothesis explains carbon export efficiency observations in the southern ocean. *Geophysical Research Letters*, *44*(4), 1831–1838. https://doi.org/10.1002/2016gl072378

Browning, T. J., & Moore, C. M. (2023). Global analysis of ocean phytoplankton nutrient limitation reveals high prevalence of co-limitation. *Nature Communications*, *14*(1), 5014. https://doi.org/10.1038/s41467-023-40774-0

Brzezinski, M. A., Baines, S. B., Balch, W. M., Beucher, C. P., Chai, F., Dugdale, R. C., et al. (2011). Co-limitation of diatoms by iron and silicic acid in the equatorial pacific. *Deep Sea Research Part II: Topical Studies in Oceanography*, *58*(3–4), 493–511. https://doi.org/10.1016/j.dsr2.2010.08.005

Brzezinski, M. A., Dickson, M.-L., Nelson, D. M., & Sambrotto, R. (2003). Ratios of si, c and n uptake by microplankton in the southern ocean. *Deep Sea Research Part II: Topical Studies in Oceanography*, *50*(3–4), 619–633. https://doi.org/10.1016/s0967-0645(02)00587-8

Brzezinski, M. A., Krause, J. W., Bundy, R. M., Barbeau, K. A., Franks, P., Goericke, R., et al. (2015). Enhanced silica ballasting from iron stress sustains carbon export in a frontal zone within the c alifornia c urrent. *Journal of Geophysical Research: Oceans*, *120*(7), 4654–4669. https://doi.org/10.1002/2015jc010829

Brzezinski, M. A., Olson, R. J., & Chisholm, S. W. (1990). Silicon availability and cell-cycle progression in marine diatoms. *Marine Ecology Progress Series*, *67*, 83–96. https://doi.org/10.3354/meps067083

19448007, 2024, 19, Downloaded from https://agupubs.onlinelibrary.wiley.com/doi/10.1029/2024GL110225 by University Of Southampton, Wiley Online Library on [15/10/2024]. See the Terms and Conditions (https://onlinelibrary.wiley.com/terms-and-conditions) on Wiley Online Library for rules of use; OA articles are governed by the applicable Creative Commons License

Buitenhuis, E. T., Guest, J. K., Wright, R., Townsend, P., & Le Quéré, C. (2023). *Zenodo*. Retrieved from https://doi.org/10.5281/ZENODO.8388158. Description of the planktom equations

Buitenhuis, E. T., Le Quere, C., Bednaršek, N., & Schiebel, R. (2019). Large contribution of pteropods to shallow caco3 export. *Global Biogeochemical Cycles*, *33*(3), 458–468. https://doi.org/10.1029/2018gb006110

Cael, B. (2021). Variability-based constraint on ocean primary production models. *Limnology and Oceanography Letters*, *6*(5), 262–269. https://doi.org/10.1002/lol2.10196

Cael, B. B. (2024). *Code for a global ocean ballasting-silicate relationship*. Zenodo. Retrieved from https://zenodo.org/doi/10.5281/zenodo.13303336

Cael, B., Bisson, K., Conte, M., Duret, M. T., Follett, C. L., Henson, S. A., et al. (2021). Open ocean particle flux variability from surface to seafloor. *Geophysical Research Letters*, *48*(9), e2021GL092895. https://doi.org/10.1029/2021gl092895

Cael, B., Bisson, K., & Follett, C. L. (2018). Can rates of ocean primary production and biological carbon export be related through their probability distributions? *Global Biogeochemical Cycles*, *32*(6), 954–970. https://doi.org/10.1029/2017gb005797

Charette, M. A., & Smith, W. H. (2010). The volume of earth's ocean. *Oceanography*, *23*(2), 112–114. https://doi.org/10.5670/oceanog.2010.51

Cram, J. A., Weber, T., Leung, S. W., McDonnell, A. M., Liang, J.-H., & Deutsch, C. (2018). The role of particle size, ballast, temperature, and oxygen in the sinking flux to the deep sea. *Global Biogeochemical Cycles*, *32*(5), 858–876. https://doi.org/10.1029/2017gb005710

DeVries, T., Primeau, F., & Deutsch, C. (2012). The sequestration efficiency of the biological pump. *Geophysical Research Letters*, *39*(13). https://doi.org/10.1029/2012gl051963

Ducklow, H. W., Steinberg, D. K., & Buesseler, K. O. (2001). Upper ocean carbon export and the biological pump. *Oceanography*, *14*(4), 50–58. https://doi.org/10.5670/oceanog.2001.06

Efron, B., & Tibshirani, R. (1986). Bootstrap methods for standard errors, confidence intervals, and other measures of statistical accuracy. *Statistical Science*, *1*(1), 54–75. https://doi.org/10.1214/ss/1177013815

Franck, V. M., Brzezinski, M. A., Coale, K. H., & Nelson, D. M. (2000). Iron and silicic acid concentrations regulate si uptake north and south of the polar frontal zone in the pacific sector of the southern ocean. *Deep Sea Research Part II: Topical Studies in Oceanography*, *47*(15–16), 3315–3338. https://doi.org/10.1016/s0967-0645(00)00070-9

Francois, R., Honjo, S., Krishfield, R., & Manganini, S. (2002). Factors controlling the flux of organic carbon to the bathypelagic zone of the ocean. *Global Biogeochemical Cycles*, *16*(4), 34–41. https://doi.org/10.1029/2001gb001722

Garcia, H., Weathers, K., Paver, C., Smolyar, I., Boyer, T., Locarnini, M., et al. (2019). World ocean atlas 2018. vol. 4: Dissolved inorganic nutrients (phosphate, nitrate and nitrate+ nitrite, silicate).

Gnanadesikan, A. (1999). A global model of silicon cycling: Sensitivity to eddy parameterization and dissolution. *Global Biogeochemical Cycles*, *13*(1), 199–220. https://doi.org/10.1029/1998gb900013

Griffiths, J. D., Barker, S., Hendry, K. R., Thornalley, D. J., Van De Flierdt, T., Hall, I. R., & Anderson, R. F. (2013). Evidence of silicic acid leakage to the tropical atlantic via antarctic intermediate water during marine isotope stage 4. *Paleoceanography*, *28*(2), 307–318. https://doi.org/10.1002/palo.20030

Heinze, C., Eyring, V., Friedlingstein, P., Jones, C., Balkanski, Y., Collins, W., et al. (2019). Esd reviews: Climate feedbacks in the earth system and prospects for their evaluation. *Earth System Dynamics*, *10*(3), 379–452. https://doi.org/10.5194/esd-10-379-2019

Henson, S. A., Laufkötter, C., Leung, S., Giering, S. L., Palevsky, H. I., & Cavan, E. L. (2022). Uncertain response of ocean biological carbon export in a changing world. *Nature Geoscience*, *15*(4), 248–254. https://doi.org/10.1038/s41561-022-00927-0

Henson, S. A., Sanders, R., & Madsen, E. (2012). Global patterns in efficiency of particulate organic carbon export and transfer to the deep ocean. *Global Biogeochemical Cycles*, *26*(1). https://doi.org/10.1029/2011gb004099

Holzer, M., Primeau, F. W., DeVries, T., & Matear, R. (2014). The southern ocean silicon trap: Data-constrained estimates of regenerated silicic acid, trapping efficiencies, and global transport paths. *Journal of Geophysical Research: Oceans*, *119*(1), 313–331. https://doi.org/10.1002/2013jc009356

Hutchins, D. A., & Bruland, K. W. (1998). Iron-limited diatom growth and si: N uptake ratios in a coastal upwelling regime. *Nature*, *393*(6685), 561–564. https://doi.org/10.1038/31203

Jin, X., Gruber, N., Dunne, J., Sarmiento, J. L., & Armstrong, R. (2006). Diagnosing the contribution of phytoplankton functional groups to the production and export of particulate organic carbon, caco3, and opal from global nutrient and alkalinity distributions. *Global Biogeochemical Cycles*, *20*(2). https://doi.org/10.1029/2005gb002532

Klaas, C., & Archer, D. E. (2002). Association of sinking organic matter with various types of mineral ballast in the deep sea: Implications for the rain ratio. *Global Biogeochemical Cycles*, *16*(4), 63–71. https://doi.org/10.1029/2001gb001765

Le Quéré, C., Buitenhuis, E. T., Moriarty, R., Alvain, S., Aumont, O., Bopp, L., et al. (2016). Role of zooplankton dynamics for southern ocean phytoplankton biomass and global biogeochemical cycles. *Biogeosciences*, *13*(14), 4111–4133. https://doi.org/10.5194/bg-13-4111-2016

Malviya, S., Scalco, E., Audic, S., Vincent, F., Veluchamy, A., Poulain, J., et al. (2016). Insights into global diatom distribution and diversity in the world's ocean. *Proceedings of the National Academy of Sciences*, *113*(11), E1516–E1525. https://doi.org/10.1073/pnas.1509523113

Marchetti, A., Varela, D. E., Lance, V. P., Lance, V. P., Palmucci, M., Giordano, M., & Virginia Armbrust, E. (2010). Iron and silicic acid effects on phytoplankton productivity, diversity, and chemical composition in the central equatorial pacific ocean. *Limnology & Oceanography*, *55*(1), 11–29. https://doi.org/10.4319/lo.2010.55.1.0011

Marsay, C. M., Sanders, R. J., Henson, S. A., Pabortsava, K., Achterberg, E. P., & Lampitt, R. S. (2015). Attenuation of sinking particulate organic carbon flux through the mesopelagic ocean. *Proceedings of the National Academy of Sciences*, *112*(4), 1089–1094. https://doi.org/10.1073/pnas.1415311112

Martin, J. H., Knauer, G. A., Karl, D. M., & Broenkow, W. W. (1987). Vertex: Carbon cycling in the northeast pacific. *Deep-Sea Research, Part A: Oceanographic Research Papers*, *34*(2), 267–285. https://doi.org/10.1016/0198-0149(87)90086-0

Martin-Jézéquel, V., Hildebrand, M., & Brzezinski, M. A. (2000). Silicon metabolism in diatoms: Implications for growth. *Journal of Phycology*, *36*(5), 821–840. https://doi.org/10.1046/j.1529-8817.2000.00019.x

Matsumoto, K., & Sarmiento, J. L. (2008). A corollary to the silicic acid leakage hypothesis. *Paleoceanography*, *23*(2). https://doi.org/10.1029/2007pa001515

Matsumoto, K., Sarmiento, J. L., & Brzezinski, M. A. (2002). Silicic acid leakage from the southern ocean: A possible explanation for glacial atmospheric pco2. *Global Biogeochemical Cycles*, *16*(3), 1–5. https://doi.org/10.1029/2001gb001442

Matsumoto, K., Tokos, K., Huston, A., & Joy-Warren, H. (2013). Mesmo 2: A mechanistic marine silica cycle and coupling to a simple terrestrial scheme. *Geoscientific Model Development*, *6*(2), 477–494. https://doi.org/10.5194/gmd-6-477-2013

Montroll, E. W., & Shlesinger, M. F. (1982). On 1/f noise and other distributions with long tails. *Proceedings of the National Academy of Sciences*, *79*(10), 3380–3383. https://doi.org/10.1073/pnas.79.10.3380

19448007, 2024, 19, Downloaded from https://agupubs.onlinelibrary.wiley.com/doi/10.1029/2024GL110225 by University Of Southampton, Wiley Online Library on [15/10/2024]. See the Terms and Conditions (https://onlinelibrary.wiley.com/terms-and-conditions) on Wiley Online Library for rules of use; OA articles are governed by the applicable Creative Commons License

Mouw, C. B., Barnett, A., McKinley, G. A., Gloege, L., & Pilcher, D. (2016). Global ocean particulate organic carbon flux merged with satellite parameters. *Earth System Science Data*, *8*(2), 531–541. https://doi.org/10.5194/essd-8-531-2016

Pančić, M., Torres, R. R., Almeda, R., & Kiørboe, T. (2019). Silicified cell walls as a defensive trait in diatoms. *Proceedings of the Royal Society B*, *286*(1901), 20190184. https://doi.org/10.1098/rspb.2019.0184

Pasquier, B., & Holzer, M. (2017). Inverse-model estimates of the ocean's coupled phosphorus, silicon, and iron cycles. *Biogeosciences*, *14*(18), 4125–4159. https://doi.org/10.5194/bg-14-4125-2017

Petrou, K., Baker, K. G., Nielsen, D. A., Hancock, A. M., Schulz, K. G., & Davidson, A. T. (2019). Acidification diminishes diatom silica production in the southern ocean. *Nature Climate Change*, *9*(10), 781–786. https://doi.org/10.1038/s41558-019-0557-y

Pichevin, L., Ganeshram, R., Geibert, W., Thunell, R., & Hinton, R. (2014). Silica burial enhanced by iron limitation in oceanic upwelling margins. *Nature Geoscience*, *7*(7), 541–546. https://doi.org/10.1038/ngeo2181

Pondaven, P., Gallinari, M., Chollet, S., Bucciarelli, E., Sarthou, G., Schultes, S., & Jean, F. (2007). Grazing-induced changes in cell wall silicification in a marine diatom. *Protist*, *158*(1), 21–28. https://doi.org/10.1016/j.protis.2006.09.002

Qiu, B., & Huang, R. X. (1995). Ventilation of the north atlantic and North Pacific: Subduction versus obduction. *Journal of Physical Oceanography*, *25*(10), 2374–2390. https://doi.org/10.1175/1520-0485(1995)025<2374:votnaa>2.0.co;2

Round, F. E., Crawford, R. M., & Mann, D. G. (1990). *Diatoms: Biology and morphology of the genera*. Cambridge university press.

Ryderheim, F., Grønning, J., & Kiørboe, T. (2022). Thicker shells reduce copepod grazing on diatoms. *Limnology and Oceanography Letters*, *7*(5), 435–442. https://doi.org/10.1002/lol2.10243

Saha, S., Moorthi, S., Pan, H.-L., Wu, X., Wang, J., Nadiga, S., et al. (2010). The ncep climate forecast system reanalysis. *Bulletin of the American Meteorological Society*, *91*(8), 1015–1058. https://doi.org/10.1175/2010bams3001.1

Sarmiento, J. L., Gruber, N., Brzezinski, M., & Dunne, J. (2004). High-latitude controls of thermocline nutrients and low latitude biological productivity. *Nature*, *427*(6969), 56–60. https://doi.org/10.1038/nature02127

Sarmiento, J. L., Simeon, J., Gnanadesikan, A., Gruber, N., Key, R., & Schlitzer, R. (2007). Deep ocean biogeochemistry of silicic acid and nitrate. *Global Biogeochemical Cycles*, *21*(1). https://doi.org/10.1029/2006gb002720

Siegel, D., DeVries, T., Doney, S., & Bell, T. (2021). Assessing the sequestration time scales of some ocean-based carbon dioxide reduction strategies. *Environmental Research Letters*, *16*(10), 104003. https://doi.org/10.1088/1748-9326/ac0be0

Takeda, S. (1998). Influence of iron availability on nutrient consumption ratio of diatoms in oceanic waters. *Nature*, *393*(6687), 774–777. https://doi.org/10.1038/31674

Tréguer, P., Bowler, C., Moriceau, B., Dutkiewicz, S., Gehlen, M., Aumont, O., et al. (2018). Influence of diatom diversity on the ocean biological carbon pump. *Nature Geoscience*, *11*(1), 27–37. https://doi.org/10.1038/s41561-017-0028-x

Wilson, J. D., Barker, S., & Ridgwell, A. (2012). Assessment of the spatial variability in particulate organic matter and mineral sinking fluxes in the ocean interior: Implications for the ballast hypothesis. *Global Biogeochemical Cycles*, *26*(4). https://doi.org/10.1029/2012gb004398

Wright, R. M., Le Quéré, C., Buitenhuis, E., Pitois, S., & Gibbons, M. J. (2021). Role of jellyfish in the plankton ecosystem revealed using a global ocean biogeochemical model. *Biogeosciences*, *18*(4), 1291–1320. https://doi.org/10.5194/bg-18-1291-2021

19448007, 2024, 19, Downloaded from https://agupubs.onlinelibrary.wiley.com/doi/10.1029/2024GL110225 by University Of Southampton, Wiley Online Library on [15/10/2024]. See the Terms and Conditions (https://onlinelibrary.wiley.com/terms-and-conditions) on Wiley Online Library for rules of use; OA articles are governed by the applicable Creative Commons License